Enhanced efficiency of CsPbBr$_3$ perovskite solar cells with doping MgBr$_2$

LINGHAO WU[1], FEI ZHAO[1,*], PEIZHI YANG[2]
[1]School of Photoelectric Engineering, Changzhou Institute of Technology, Changzhou, Jiangsu, 213032, China
[2]Key Laboratory of Advanced Technique & Preparation for Renewable Energy Materials, Ministry of Education, Yunnan Normal University, Kunming 650500, China

The all-inorganic CsPbBr$_3$ perovskite solar cell without electron-hole transport layer has attracted widespread attention from researchers due to its simplified process, reduced costs and excellent air stability. However, its photoelectric conversion efficiency is currently relatively low. Here, the CsPbBr$_3$ perovskite thin film with doping MgBr$_2$ is used as a novel absorber for all-inorganic carbon-based perovskite solar cell. There is no significant change in the optical band gap of CsPbBr$_3$ after the incorporation of MgBr$_2$. However, doping MgBr$_2$ can effectively enhance the crystallinity of CsPbBr$_3$ thin film and improve carrier separation capability of CsPbBr$_3$ perovskite cell. Compared with the CsPbBr$_3$ perovskite cell without doping MgBr$_2$, the efficiency of the CsPbBr$_3$ perovskite cell with doping MgBr$_2$ increases from 1.79% to 2.30%. This work provides a novel pathway for preparing highly-efficient CsPbBr$_3$ perovskite solar cell.

1. Introduction

In the past decade, the photovoltaic conversion efficiency of organic-inorganic hybrid perovskite solar cells has increased from 3.8% to over 26% [1-3]. The structure of organic-inorganic hybrid perovskite solar cell mainly includes front electrode, electron transport layer, perovskite absorption layer, hole transport layer, and back electrode. Organic-inorganic hybrid perovskite solar cells are prone to rapid decomposition in the air, leading to a sharp decrease in the photoelectric conversion efficiency of device [4]. The reason behind this phenomenon is due to the instability of organic-inorganic hybrid perovskite thin films. Organic components are present in organic-inorganic hybrid perovskite thin films, which can cause rapid decomposition of perovskite thin films in air. In order to suppress the decomposition of perovskite thin films, inorganic components can be used to replace the organic components in organic-inorganic hybrid perovskite thin films, forming all-inorganic perovskite thin film.

All-inorganic perovskite thin films have received widespread attention due to their excellent air stability [5-7]. All-inorganic perovskite thin films mainly include CsPbI$_3$ [8], CsPbIBr$_2$ [9], CsPbI$_2$Br [10], and CsPbBr$_3$ [11]. Among these all-inorganic perovskite thin films, CsPbBr$_3$ perovskite thin films have the optical band gap of 2.3 eV and the best air stability, making them very suitable as the absorption layer of top cell in tandem solar cells [12]. Therefore, the preparation of high-quality

CsPbBr$_3$ perovskite thin films is of great scientific significance. At present, the main preparation techniques for CsPbBr$_3$ perovskite thin films include thermal evaporation and solution spin coating. The CsPbBr$_3$ perovskite thin film prepared by thermal evaporation method has good uniformity. However, the preparation cost of this method is relatively high. All-inorganic CsPbBr$_3$ perovskite thin films with good uniformity can also be prepared by solution spin coating method. Meanwhile, the preparation cost of this method is relatively low. Therefore, solution spin coating method is a more practical thin film preparation technique.

In order to further improve the growth quality of CsPbBr$_3$ perovskite thin films, it is necessary to find a more effective method based on the CsPbBr$_3$ perovskite thin films prepared by solution spin coating method. According to some literature reports, element doping strategies can effectively improve the growth quality of CsPbBr$_3$ perovskite thin films [13,14]. At present, the elements doped into CsPbBr$_3$ perovskite thin films include Yb, Er, Ho, Tb, and Sm [15]. The CsPbBr$_3$ perovskite thin films doped by these elements are applied in the field of solar cells with electron-hole transport layers, and can all achieve efficiency improvement. However, the electron-hole transport layers often have a high price, which further increases the preparation cost of the device. Thus, it is very important to study element-doped CsPbBr$_3$ perovskite solar cells without electron-hole transport layers. However, to our knowledge, there are currently no relevant reports on the

effect of doping $MgBr_2$ on the performance of $CsPbBr_3$ perovskite solar cells without electron-hole transport layers. Therefore, there is an urgent need to explore the performance of $MgBr_2$-doped $CsPbBr_3$ perovskite solar cells without electron-hole transport layers.

In this work, $MgBr_2$-doped $CsPbBr_3$ perovskite solar cells were successfully prepared. The structure and optical properties of $MgBr_2$-doped $CsPbBr_3$ perovskite thin films and photovoltaic performance of corresponding devices were systematically studied. The results indicate that doping $MgBr_2$ can improve the crystallinity of $CsPbBr_3$ perovskite thin film and enhance its carrier separation capability. The efficiency of the $MgBr_2$-doped $CsPbBr_3$ perovskite cell is higher (2.30%) in comparison to the undoped $CsPbBr_3$ perovskite cell (1.79%).

2. Experimental

2.1. Preparation of devices

FTO substrates were successively cleaned by isopropanol, ethanol and deionized water. For preparing $CsPbBr_3$ perovskite thin films without doping $MgBr_2$, the $CsPbBr_3$ thin films were prepared on the FTO substrates using a multi-step spin coating technology. N, N-dimethylformamide (DMF) solution containing $PbBr_2$ powder (mass concentration of 367 mg/ml) was spin-coated on the FTO substrates to form the $PbBr_2$ thin films. The spin-coating speed and spin-coating time for preparing $PbBr_2$ thin films are 2000 rpm and 30 s, respectively. Afterwards, the $PbBr_2$ thin film was placed on a heating table for annealing treatment. The annealing temperature and annealing time of $PbBr_2$ thin films are 90 ℃ and 30 min, respectively. The methanol solution with CsBr powder (mass concentration of 15 mg/mL) was rapidly spin-coated on $PbBr_2$ thin films. The spin-coating speed and spin-coating time of the methanol solution with CsBr powder are set to 2000 rpm and 30 s, respectively. The methanol solution of CsBr was spin-coated four times. Then, each layer of CsBr methanol solution were heated at 250 ℃ for 5 min. Finally, the $CsPbBr_3$ perovskite thin films was successfully synthesized. For depositing $CsPbBr_3$ perovskite thin film with doping $MgBr_2$, different qualities of $MgBr_2$ powder (6 mg and 10 mg) were added to 1 ml DMF solution containing $PbBr_2$. The other steps are consistent with the corresponding synthesis steps of the undoped $CsPbBr_3$ thin film. Finally, a carbon back-electrode was deposited on the perovskite film by coating commercial carbon paste.

2.2. Characterizations

The structure of the sample was measured by the X-ray diffraction (XRD) diffractometer. The morphology of the samples was evaluated by field emission scanning electron microscopy (SEM). The grain size of the sample was tested from SEM images and a nano-measurement software. The valence states of elements were obtained via X-ray photoelectron spectroscopy (XPS) spectra. Ultraviolet-visible (UV-vis) absorption spectra of the samples were characterized to gain their optical band gap. The PL spectra were tested on a spectrofluorometer excited by 325 nm laser. The J-V curves were measured using a solar simulator under AM 1.5G simulated solar illumination. A black mask with 0.09 cm^2 area was used on the surface of cell to avoid stray light.

3. Results and discussions

3.1. Analysis of structure

Fig. 1a shows the XRD spectra of $CsPbBr_3$ perovskite thin films without and with doping $MgBr_2$. According to the XRD spectra, two obvious diffraction peaks appeared at 21.68° and 30.77°. Two diffraction peaks correspond to the (110) and (200) crystal planes of $CsPbBr_3$ thin films, respectively [16]. In addition, there is a weak diffraction peak at 26.54°, which corresponds to FTO. Among the two diffraction peaks of the (110) and (200) crystal planes for all $CsPbBr_3$ samples, the diffraction peak intensity of the (110) crystal plane is the highest, indicating that the samples undergo preferential orientation growth during the growth process [17]. Fig. 1b indicates enlarged XRD images of all samples. Compared with the $CsPbBr_3$ perovskite thin films without doping $MgBr_2$, the diffraction peak intensity of the (110) crystal plane of the $CsPbBr_3$ thin film with doping $MgBr_2$ is higher, indicating enhanced crystallinity of the $CsPbBr_3$ thin film [18,19]. The enhancement of the crystallinity is beneficial for improving the photovoltaic performance of the solar cells. In addition, it can be observed from Fig. 1b that after doping $MgBr_2$, the diffraction peak of the (110) crystal plane for $CsPbBr_3$ shifts towards a larger angle direction. This is because Mg ions have already been doped into the lattice of the $CsPbBr_3$ thin film.
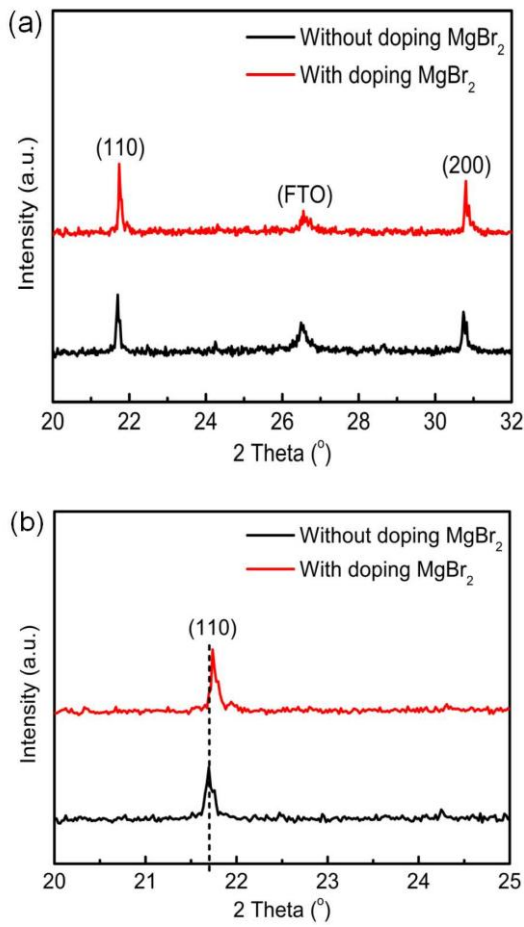
Fig. 1. (a) XRD spectra of the CsPbBr₃ perovskite thin films without and with doping MgBr₂. (b) Partial enlarged XRD spectra of CsPbBr₃ perovskite thin films without and with doping MgBr₂ (colour online)

3.2. Elemental valence state and morphology characterization

Fig. 2a shows the XPS (Pb 4f) spectra of CsPbBr₃ perovskite thin films without and with doping MgBr₂. Compared with the undoped CsPbBr₃ perovskite thin film, the characteristic peak of MgBr₂-doped CsPbBr₃ perovskite thin film shows a red shift. This directly proves that Mg ions have been doped into the lattice of CsPbBr₃ perovskite thin films [14], which is consistent with previous analysis results. Fig. 2b indicates the XPS (Mg 1s) spectra of CsPbBr₃ perovskite thin films with doping MgBr₂. As shown in Fig. 2b, the diffraction peak further proves that Mg ions have successfully entered the perovskite lattice.
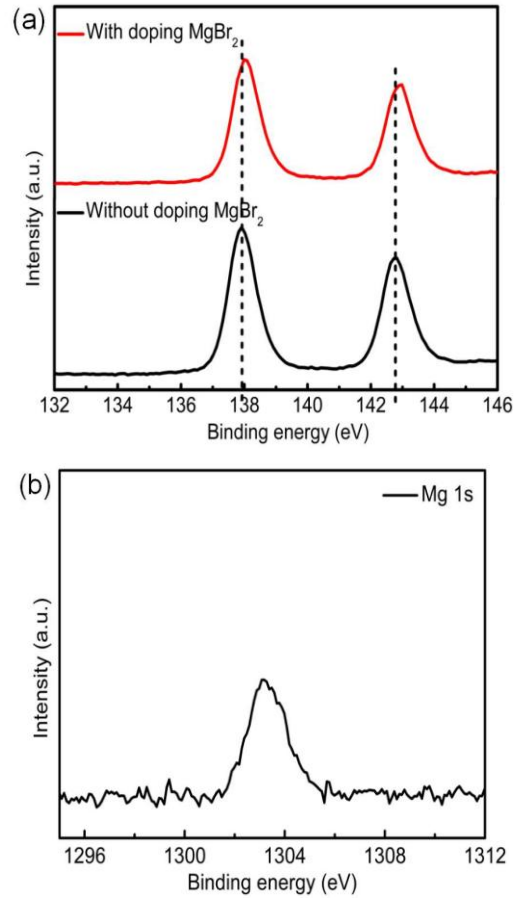

Fig. 2. (a) XPS spectra (Pb 4f) of the CsPbBr₃ perovskite thin films without and with doping MgBr₂. (b) XPS spectra (Mg 1s) of the CsPbBr₃ perovskite thin films with doping MgBr₂ (colour online)

Fig. 3a and 3b show the SEM surface morphology of CsPbBr₃ perovskite thin films without and with doping MgBr₂. Compared with undoped CsPbBr₃ perovskite thin films, the grains of MgBr₂-doped CsPbBr₃ perovskite thin films are larger and the number of their grain boundaries is fewer. Meanwhile, the grain growth is more uniform and denser. These results are beneficial for improving the photovoltaic performance of CsPbBr₃ solar cells [20]. Furthermore, we calculated the average size of CsPbBr₃ grains. The average grain sizes of CsPbBr₃ perovskite thin films without and with doping MgBr₂ are 569 nm and 678 nm, separately. This is consistent with our previous analysis results.
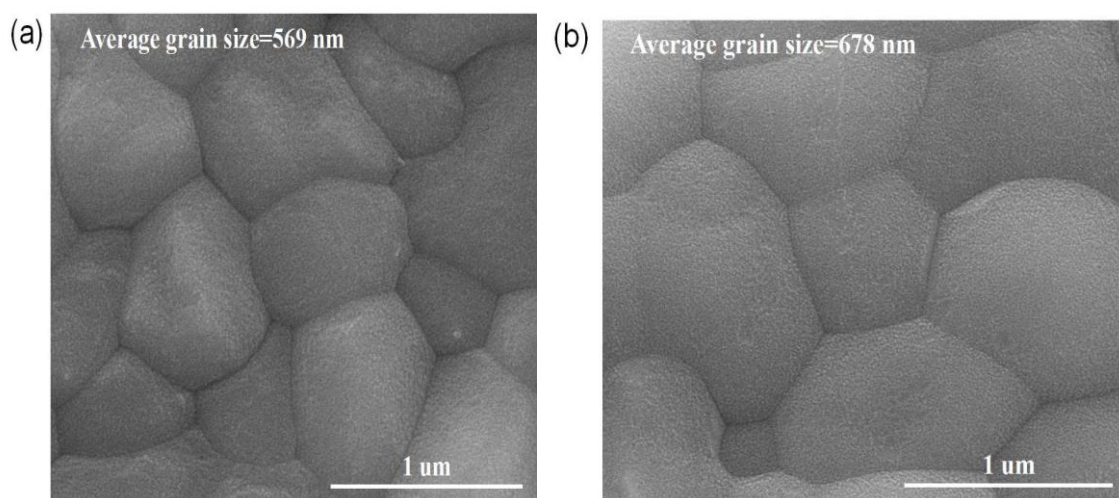
Fig. 3. SEM images of the CsPbBr₃ perovskite thin films (a) without doping MgBr₂ and (b) with doping MgBr₂

3.3. Analysis of optical performance

Fig. 4a shows the optical absorption spectra of $CsPbBr_3$ perovskite thin films without and with doping $MgBr_2$. The light absorption intensity of $CsPbBr_3$ perovskite thin film with doping $MgBr_2$ is higher in comparison to undoped $CsPbBr_3$ perovskite thin film. This indicates that using $MgBr_2$-doped $CsPbBr_3$ perovskite thin film as the absorption layer of solar cell can absorb more sunlight [14]. The reason of the absorption intensity improvement for $MgBr_2$-doped $CsPbBr_3$ thin films is due to their higher crystallinity. Fig. 4b indicates the relationship between $(ahv)^2$ and hv. Based on the relationship between $(ahv)^2$ and hv, the optical band gap of the $CsPbBr_3$ thin film can be determined. Compared with undoped $CsPbBr_3$ thin film, the optical band gap of $MgBr_2$-doped $CsPbBr_3$ thin film shows no significant change.

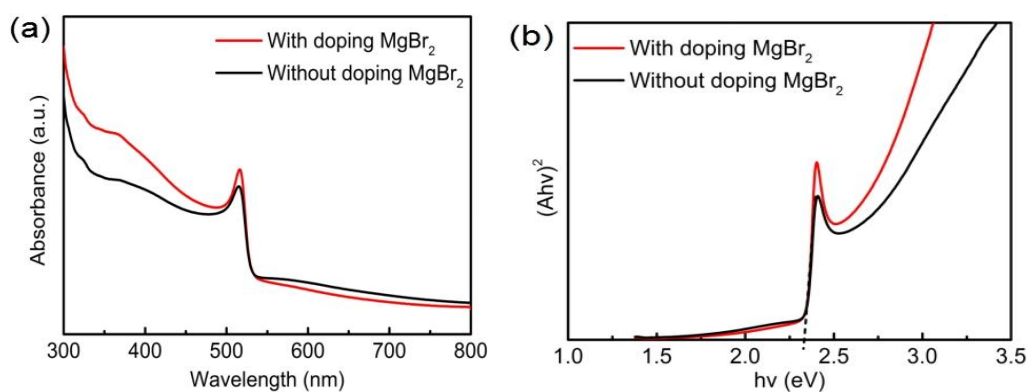*Fig. 4. (a) Ultraviolet visible light absorption spectra of the CsPbBr₃ perovskite thin films without and with doping MgBr₂. (b) Plot of $(ahv)^2$ versus hv for the estimation of the band gap energy of the CsPbBr₃ perovskite thin films (colour online)*

Fig. 5 shows the PL spectra of the $CsPbBr_3$ perovskite thin films without and with doping $MgBr_2$. From Fig. 5, it can be seen that all samples exhibit a clear luminescent peak at ~526 nm. However, compared with the undoped $CsPbBr_3$ perovskite thin film, the $MgBr_2$-doped $CsPbBr_3$ perovskite film has a higher luminescence peak intensity, indicating a stronger ability to separate electrons and holes.

The enhancement of electron and hole separation ability can promote the collection of electron and hole at both ends of FTO and carbon electrodes, thereby improving the photovoltaic performance of $CsPbBr_3$ solar cell [21].
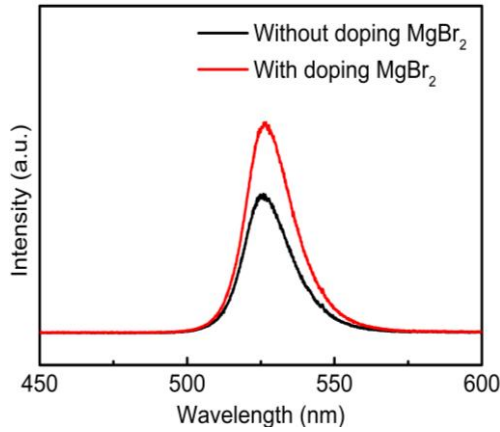
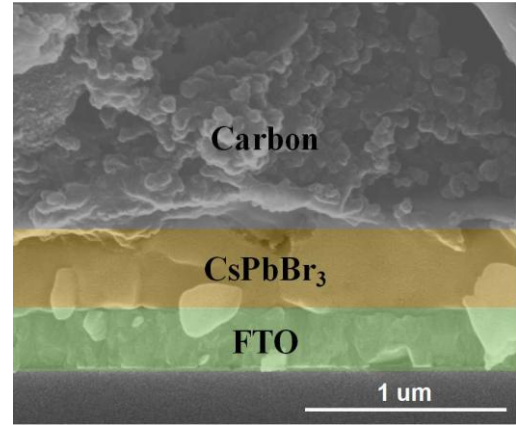Fig. 5. PL spectra of the CsPbBr₃ perovskite thin films without and with doping MgBr₂ (colour online)

Fig. 6. Structural diagram of the simplified CsPbBr₃ perovskite device (colour online)

3.4. Analysis of device structure and its photovoltaic performance

Fig. 6 indicates the structural diagram of the simplified CsPbBr₃ perovskite device. The structure of CsPbBr₃ perovskite solar cell includes FTO electrode, CsPbBr₃ absorption layer and carbon electrode. There are no obvious pores at the interfaces of FTO/CsPbBr₃ and C/CsPbBr₃, indicating a close contact between them. This can effectively reduce interface defects and have a positive impact on the photovoltaic performance of CsPbBr₃ solar cells [22].

Fig. 7 shows the J-V curves of the CsPbBr₃ perovskite device with different MgBr₂ concentrations. When the doping concentration of MgBr₂ increases to 6 mg, the open circuit voltage (V_{oc}), short circuit current density (J_{sc}), fill factor (FF), and efficiency of CsPbBr₃ cell are effectively improved. However, the V_{oc}, J_{sc}, FF, and efficiency of CsPbBr₃ cell decrease comprehensively after the doping MgBr₂ concentration continues to increase to 10mg.
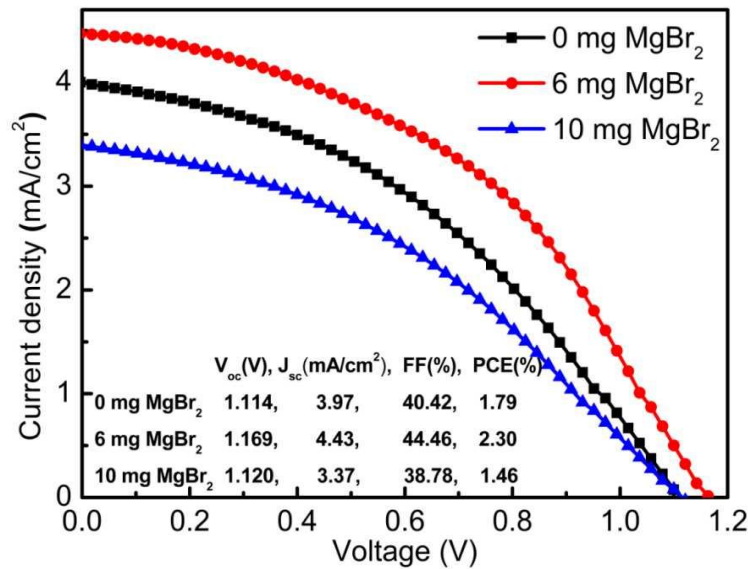

Fig. 7. J-V curves of the CsPbBr₃ perovskite device with different MgBr₂ concentrations (colour online)

Therefore, when the doping MgBr₂ concentration is 6 mg, the photovoltaic performance of CsPbBr₃ cells is the best. The V_{oc}, J_{sc}, FF and efficiency of the undoped CsPbBr₃ devices are 1.114 V, 3.97 mA/cm², 40.42%, and 1.79%, respectively. However, the CsPbBr₃ device achieves a V_{oc} of 1.169 V, a J_{sc} of 4.43 mA/cm², a FF of 44.46% and an efficiency of 2.30% after doping 6 mg MgBr₂. This indicates that doping MgBr₂ can improve the photovoltaic performance of CsPbBr₃ cells. The improvement in photovoltaic performance of CsPbBr₃

cell is attributed to the enhanced crystallinity of $CsPbBr_3$ absorbers, its increased absorption rate, and its improved separation ability of electron and hole [23], which is consistent with previous analysis results.

4. Conclusions

Simplified all-inorganic $CsPbBr_3$ perovskite solar cells based on doping $MgBr_2$ have been successfully prepared. Some experimental results can be obtained through XRD, XPS, SEM, PL, absorption spectrum and J-V curve. It is found that Mg element is incorporated into $CsPbBr_3$ according to the result of XRD and XPS. The V_{oc}, J_{sc} and FF of the $CsPbBr_3$ device with doping $MgBr_2$ are enhanced due to the crystallinity improvement and the carrier separation capability improvement. The best efficiency of all-inorganic $CsPbBr_3$ device is increased from 1.79% to 2.30% after doping $MgBr_2$. This work brings a novel approach to the preparation of highly-efficient $CsPbBr_3$ perovskite solar cell.

References

[1] Z. Zhang, R. Zhu, Y. Tang, Z. Su, S. Hu, X. Zhang, J. Zhang, J. Zhao, Y. Xue, X. Gao, G. Li, J. Pascual, A. Abate, M. Li, Adv. Mater. **36**, 2312264 (2024).

[2] U. Khan, A. Rauf, S. Feng, A. R. Akbar, G. Peng, Q. Zheng, R. Wu, M. Khan, Z. Peng, F. Liu, Chem. Commun. **153**, 110862 (2023).

[3] W. Zhang, J. Xiong, J. Li, W. A. Daoud, Small **16**, 2001535 (2020).

[4] P. Luo, Y. Zhou, S. Zhou, Y. Lu, C. Xu, W. Xia, L. Sun, Chem. Eng. J. **343**, 146 (2018).

[5] H. Yuan, Y. Zhao, J. Duan, B. He, Z. Jiao, Q. Tang, Electrochim. Acta **279**, 84 (2018).

[6] J. Zhu, B. He, Z. Gong, Y. Ding, W. Zhang, X. Li, Z. Zong, H. Chen, Q. Tang, ChemSusChem **13**, 1834 (2020).

[7] Y. Xu, J. Duan, X. Yang, J. Du, Y. Wang, Y. Duan, Q. Tang, J. Mater. Chem. A **8**, 11859 (2020).

[8] Y. Guo, F. Zhao, Z. Li, J. Tao, D. Zheng, J. Jiang, J. Chu, Org. Electron. **83**, 105731 (2020).

[9] B. Yang, M. Wang, X. Hu, T. Zhou, Z. Zang, Nano Energy **57**, 718 (2019).

[10] Y. Guo, F. Zhao, J. Tao, J. Jiang, J. Zhang, J. Yang, Z. Hu, J. Chu, ChemSusChem. **12**, 983 (2019).

[11] X. Liu, X. Tan, Z. Liu, H. Ye, B. Sun, T. Shi, Z. Tang, G. Liao, Nano Energy **56**, 184 (2019).

[12] Y. Liu, B. He, J. Duan, Y. Zhao, Y. Ding, M. Tang, H. Chen, Q. Tang, J. Mater. Chem. A **7**, 12635 (2019).

[13] H. Guo, Y. Pei, J. Zhang, C. Cai, K. Zhou, Y. Zhu, J. Mater. Chem. C **7**, 11234 (2019).

[14] Y. Zhao, Y. Wang, J. Duan, X. Yang, Q. Tang, J. Mater. Chem. A **7**, 6877 (2019).

[15] J. Duan, Y. Zhao, X. Yang, Y. Wang, B. He, Q. Tang, Adv. Energy Mater. **8**(31), 1802346 (2018).

[16] F. Zhao, W. Xu, Y. Zhang, Y. Guo, P. Yang, J. Chu, Optoelectron. Adv. Mat. **18**(1-2), 39 (2024).

[17] J. Lei, F. Gao, H. Wang, J. Li, J. Jiang, X. Wu, R. Gao, Z. Yang, S. Liu, Sol. Energ. Mat. Sol. C. **187**, 1 (2018).

[18] P. Teng, X. Han, J. Li, Y. Xu, L. Kang, Y. Wang, Y. Yang, T. Yu, ACS Appl. Mater. Interfaces **10**, 9541 (2018).

[19] Y. Zhang, L. Luo, J. Hua, C. Wang, F. Huang, J. Zhong, Y. Peng, Z. Ku, Y. Cheng, Mat. Sci. Semicon. Proc. **98**, 39 (2019).

[20] F. Zhao, Y. Guo, J. Tao, Z. Li, J. Jiang, J. Chu, Appl. Optics **59**, 5481 (2020).

[21] W. Zhu, X. Yao, S. Shi, Z. Zhang, Z. Song, P. Gao, T. Wang, Y. Ba, P. Dong, ACS Appl. Energy Mater. **6**, 9798 (2023).

[22] J. Duan, Y. Zhao, B. He, Q. Tang, Small **14**, 1704443 (2018).

[23] B. Yuan, Y. Zhou, T. Liu, C. Li, B. Cao, ACS Sustainable Chem. Eng. **11**, 718 (2023).

---

*Corresponding author: fzhaobs@126.com